frontiers | Frontiers in Physics

TYPE Original Research
PUBLISHED 15 December 2022
DOI 10.3389/fphy.2022.1054778

OPEN ACCESS

EDITED BY
Guo-Bo Zhang,
National University of Defense Technology, China

REVIEWED BY
Hu Lixiang,
National University of Defense Technology, China
Ju-Kui Xue,
Northwest Normal University, China

*CORRESPONDENCE
W. P. Wang,
wangwenpeng@siom.ac.cn

†These authors have contributed equally to this work

SPECIALTY SECTION
This article was submitted to Fusion Plasma Physics, a section of the journal Frontiers in Physics

RECEIVED 27 September 2022
ACCEPTED 05 December 2022
PUBLISHED 15 December 2022

CITATION
Dong H, Wang WP, Lv ZX, Jiang C, He JZ, Leng YX, Li RX and Xu ZZ (2022), Topological structure effects of Laguerre-Gaussian laser on self-collimation acceleration mechanism. *Front. Phys.* 10:1054778. doi: 10.3389/fphy.2022.1054778

Topological structure effects of Laguerre-Gaussian laser on self-collimation acceleration mechanism

H. Dong[1,2], W. P. Wang[1]*, Z. X. Lv[1], C. Jiang[1], J. Z. He[1,2,3], Y. X. Leng[1], R. X. Li[1,3†] and Z. Z. Xu[1,3]

[1]Shanghai Institute of Optics and Fine Mechanics, Chinese Academy of Sciences (CAS), Shanghai, China, [2]University of Chinese Academy of Sciences, Beijing, China, [3]School of Physical Science and Technology, ShanghaiTech University, Shanghai, China

Energetic plasma beams can be generated through the interaction between a short-pulse high-intensity laser and solid target. However, obtaining collimated plasma beams with low divergence remains challenging. In this study, we devised a self-collimation scheme driven by a topologically structured Laguerre–Gaussian (LG) laser that irradiates a thin target in three-dimensional particle-in-cell simulations. It was observed that a high-density and narrow plasma beam could be formed by the intrinsic hollow intensity distribution of the LG laser. A magnetic tunnel was generated around the beam and collimated the plasma beam within a radius of hundreds of nanometers. This collimation can be enhanced by increasing the topological charge from l = 1 to l = 3 and then destroyed for a larger l. The collimation method is promising in applications requiring well-collimated energetic plasma beams, such as indirect drive inertial con-finement fusion, laboratory astrophysics, and radiation therapy.

KEYWORDS

Laguerre-Gaussian laser, magnetic field, collimation, plasma beam, particle-in-cell simulation

Introduction

With the advent of the multi-petawatt laser era, the laser pulse intensity can exceed 10^{22} W/cm^2 [1, 2]. When such an intense laser irradiates a solid plasma target, a large number of energetic particles are produced. In the laser-plasma interaction, the laser firstly accelerates the electrons, then the resulting space-charge field accelerates the ions. They move together as a neutral plasma beam that can propagate over a longer distance than non-neutral particle beams [3]. These plasma beams can be used for fast ignition (FI) in inertial confinement fusion [4], tumor therapy, radiographic applications, and understanding astrophysical jet phenomena. However, all these applications require the collimation or low beam divergence of the particle beam. In the FI in inertial confinement fusion, this can significantly enhance the coupling efficiency of the beam to

the compressed fusion fuel and avoid a rapid decrease in the beam intensity away from the target [5–7].

Many experiments have demonstrated that the particles (electrons and/or ions) beam has low collimation when using ultrashort high-intensity lasers [8–11]. To solve this issue, a series of simulations and experiments have been proposed to obtain an energetic particle beam with low divergence. For example, Alraddadi et al. used foam-filled resistive guide targets to achieve fast electron collimation [12]. Robinson et al. [13] used an azimuthal magnetic field pre-generated by a laser prepulse to confine the electron beam, where radially inward Lorentz forces played significant roles. Kar et al. [14] used a target with a radius of curvature to acquire a focusing ion-plasma beam. Tonican et al. [15] presented a technique for focusing ion-plasma beams using a radial electric field from a hollow microcylinder. However, these methods require rigorous target engineering or multistage acceleration schemes, which may significantly affect the stability and efficiency of most high-intensity laser-solid interactions. Therefore, a robust collimation scheme is important for various applications. In recent years, relativistic Laguerre–Gaussian (LG) lasers, which have a special structure and hollow light intensity distribution [16], have been generated experimentally [17]. A radially inward ponderomotive force can be generated from the hollow-distributed laser intensity and used to collimate the electron beam.

In this paper, we present a collimation mechanism for generating an extremely converging plasma beam. It is driven by an ultra-intense and ultrashort vortex laser with the topological charge l impinging on a solid plasma target. First, a hollow-structured plasma is formed owing to the hollow intensity distribution of the LG laser. The plasma was then concentrated toward the central axis by the radial ponderomotive force and accelerated forward by the longitudinal force. As the plasma propagates, a plasma beam with high density and current arises on the central axis. Meanwhile, the current in the plasma beam generates a strong magnetic tunnel that confines the plasma beam. Such collimation methods driven by vortex lasers can potentially be applied in a wide range of fields, such as indirect drive inertial confinement fusion, ultrafast diagnostics, and radiation therapy.

Numerical simulation and analysis

Simulation parameter

We performed 3D PIC simulations (EPOCH code [18]) to study the interaction between an ultra-intense ultrashort circularly polarized LG laser pulse and a solid plasma target. The wavelength of the laser pulse was $\lambda_0 = 0.8\,\mu$m. The laser period is $T_L = \lambda_0/c$, where c is the speed of light in vacuum. The CP LG laser can be expressed as follows:

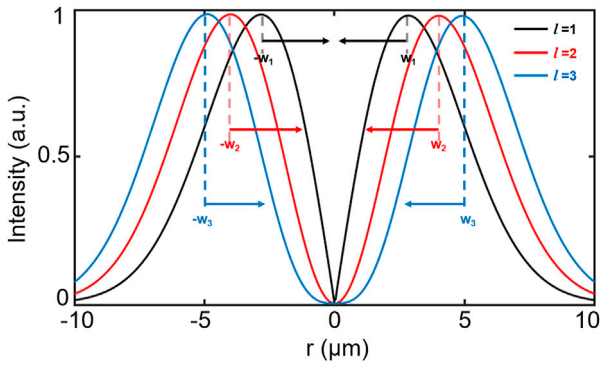

FIGURE 1
Profiles of LG laser intensity with topological l = 1, 2, and 3. The radius w_1, w_2, and w_3 correspond to the maximum light field for the topological charge of l = 1, 2, and 3.

$$E_\perp = a_0 C_l (\sqrt{2}r/w_0)^l \exp(-\sqrt{2}r/2w_0)\sin^2(\pi(x - ct)/2L)e^{i(kx-\omega t+l\varphi)}\hat{a} \quad (1)$$

where $a_0 = eE_0/m_e c\omega$, e is the electron charge, E_0 is the laser amplitude, m_e is the electron mass, ω is the laser frequency, $C_l = l^{-l/2}\exp(l/2)$ is the normalized factor of the LG laser for each order model, $r = \sqrt{y^2 + z^2}$, w_0 is the beam waist, l is the orbital angular momentum parameter, L is the pulse length in the x direction, k is the wave number, $\hat{a} = \hat{y} + i\hat{z}\sigma_z$ is the direction vector, and σ_z = -1 is the polarization parameter. For the simulations, we set a_0 = 30, w_0 = 4 μm, L = 9.9 μm, and l = 1, 2, and 3 for different topological structures of the LG laser.

The size of the simulation box was 80 μm (x) × 16 μm (y) × 16 μm (z), the number of cells was 800 × 320 × 320, and each cell was filled with two macro-electrons and two macro-protons. The mesh size is Δx = 1/10 μm and $\Delta y = \Delta z$ = 1/20 μm. The front surface of the target was located at x = 30 μm and the foil thickness was 1 μm. The foil density was $n = 30n_c$, where $n_c = \omega_L^2 m_e/4\pi e^2 = 1.1 \times 10^{21}$ cm^{-3} is the critical density. The foil was assumed to be fully ionized to protons and electrons before the laser peak arrived at the target. Notably, a micrometer plasma target can be formed by prepulse heating in the experiments [17].

Simulation analysis

The proposed self-collimation mechanism can be divided into three main stages: hole-boring, shock acceleration, and transporting stages. In the hole-boring stage [19], the laser arrives at the front surface of the target at $t = 30T_L$ and begins to interact with the plasma target. The LG laser first pushed the electrons to the back surface of the target, leaving the

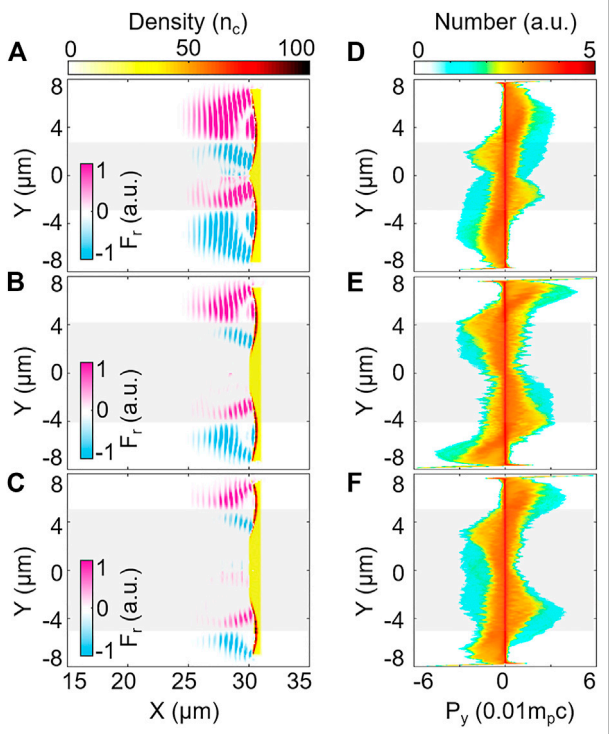

FIGURE 2
Interactions between lasers and plasma targets at $t = 50T_L$. The distribution of the electron density and LG laser ponderomotive force with topological charge **(A)** $l = 1$, **(B)** $l = 2$, **(C)** $l = 3$ are shown. The corresponding proton momentum distribution for the case with **(D)** $l = 1$, **(E)** $l = 2$, **(F)** $l = 3$ are compared. The gray bands represent the focusing regions.

heavy protons behind. Subsequently, a charged separation field between the electrons and ions is generated, accelerating the protons in the following progress [20–23]. Figure 1 shows the hollow-structured intensity distribution of an LG laser with $l = 1$, 2, and 3. This field profile generates a radial ponderomotive force that first pushes the electrons to the center axis. The resulting charge separation field between the electrons and protons then drags the protons together.

Notably, we used the normalized factor of the LG laser C_{pl} ($C_{l=1} = 1.65$, $C_{l=2} = 1.36$, $C_{l=3} = 0.86$ for $l = 1, 2, 3$) in Eq. 1 to maintain the laser intensity for research on the effects of the topological structure factor l on the plasma acceleration and collimation process. These effects are compared in Figure 1, where the maximum laser fields for $l = 1, 2, 3$ are at $w_1 = 2.83$ μm, $w_2 = 4$ μm, $w_3 = 4.9$ μm, respectively. It is assumed that the radial ponderomotive force of the LG laser plays an important role, which can be expressed as

$$F_r = \frac{-e^2}{4m_e w_0^2}\partial\frac{|E|^2}{\partial r} \quad (2)$$

where $-\partial|E|^2/\partial r = 2|E|^2(2r^2/lw_0^2\text{-}1)/r$. According to Eq. 2, the electrons can be accelerated to the central axis in the focusing region ($|r| < w_0\sqrt{|l|/2}$), which is consistent with the laser intensity distribution shown in Figure 1. In contrast, the electrons in the defocus region ($|r| > w_0\sqrt{|l|/2}$) were pushed to both sides. It was observed that a hollow-structured compressed plasma layer was formed during the hole-boring stage, where the electrons (Figures 2A–C) are first pushed toward the center axis and then drag protons (Figures 2D–F) inward by the charge separation field between the electrons and protons. As shown in Figure 2, more electrons and protons are trapped in the central region when the topological charge l increases because the size of the focusing region w_0 $w_0\sqrt{|l|/2}$ is determined by l. Notably, the laser is mostly completely reflected at $t = 50T_L$ by the compressed plasma layer formed by the laser pressure in our case. Subsequently, the plasma layer continues to travel forward and inward in the focusing region ($|r| < w_0\sqrt{|l|/2}$). For the protons, the shock acceleration mechanism plays a major role, which can be verified by calculating the Mach number $Ma = v/C_s$ during interactions, where v is the shock velocity, $C_s = \sqrt{ZK_bT_e/m_i}$ is the ion sound speed, Z is the charge number, K_bT_e is the electron temperature, and m_i is the ion mass. In the case of $l = 1$, a shock with velocity $v \approx 0.1c$ was formed at $x = 30.5$ μm at the beginning of the interaction ($t \approx 50T_L$). Figure 3A shows the features of the protons in the phase space, where the protons in front of the target are reflected by the shock. Here, the electron temperature ~1.1 MeV can be calculated from the electron energy spectrum shown in Figure 3B. Therefore, Mach number $Ma = 3$ can be obtained, which satisfies the condition of electrostatic shocks ($Ma > 1.5$) [24], so that shock acceleration occurs.

To clarify the part of the target that is collimated after the shock acceleration of the target, we divided the target into two parts: the front (30 μm $< x <$ 30.5 μm) and the back (30.5 μm $< x <$ 31 μm). Figures 3C,D show that the front protons are mainly reflected by the shock and accelerated forward. A striking high-density plasma beam is formed around the central axis at $t = 80T_L$. In contrast, the protons around the peak intensity of the LG laser are mainly accelerated, and are assumed to be partially accelerated by the target normal sheath field acceleration mechanism [25] (see Figures 3E,F). Figure 3 shows that the collimated plasma beam in our case was mainly formed from the front side of the target in the shock acceleration mechanism.

When the narrow plasma beam appears on the central axis, a negative current is formed, which can be calculated by $j = \sum n_i q_i v_i$, where i indicate particle including electron and proton, n_i is number density, q_i is electric charge, v_i is velocity of particle. Figures 4A,C show the distribution of electrons and protons. Although they have similar spatial distributions, their phase spaces are entirely different (see Figures 4B,D). The average effect of the moving electron and protons caused a negative current in the beam.

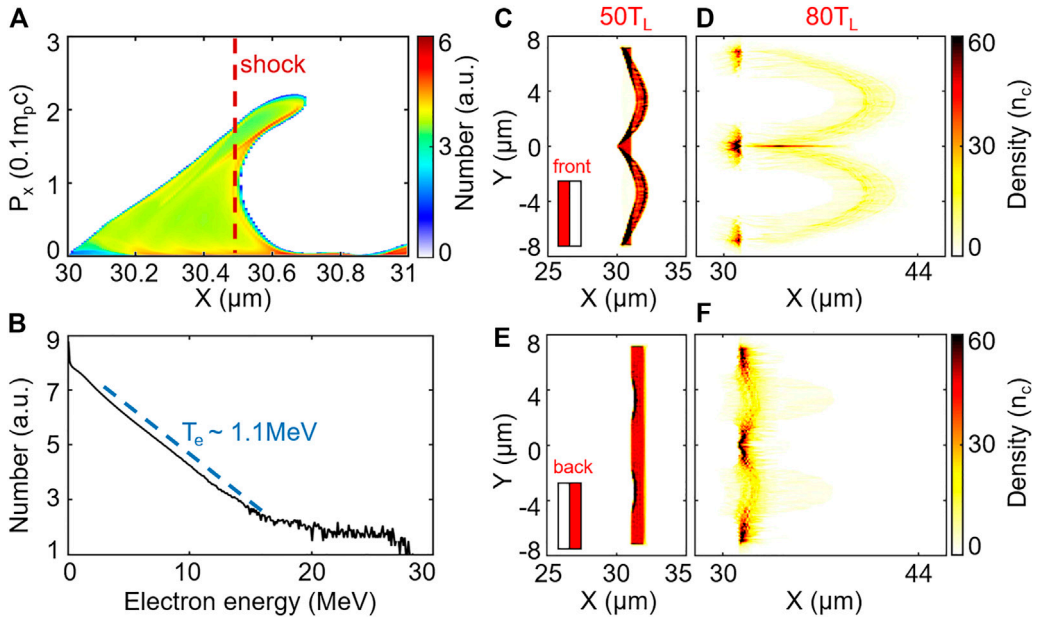

FIGURE 3
Proton acceleration in shock acceleration stage. **(A)** Proton phase space at $t = 50T_L$. The red dashed line represents the shock front. **(B)** Electron energy spectrum and electron temperature at $t = 50T_L$. Distribution of **(C,D)** the protons in the front of the target at $t = 50T_L$, $80T_L$. Distribution of **(E,F)** the protons in the back of the target at $t = 50T_L$, $80T_L$.

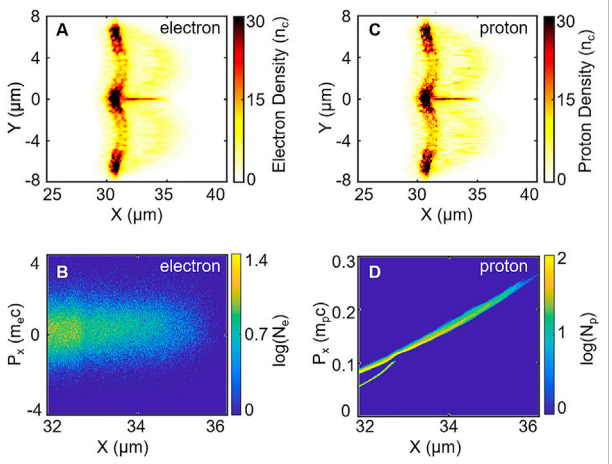

FIGURE 4
Density distribution of **(A)** the electrons and **(B)** the protons at t = 80TL. Phase spaces of **(C)** the electrons and **(D)** protons in the region (r ≤ 0.2 μm, 32 μm < x < 34 μm).

A narrow plasma beam with current is maintained for several hundred laser cycles in the transporting stage because of the self-generated magnetic field. Here, the magnetic field is assumed to be quasistatic because it is maintained for a long time, as shown in Figure 5 (right column). In the region near the target area (30 μm < x < 35 μm), the magnetic field is mainly caused by the Biermann battery effects ($\nabla n_e \times \nabla T_e$) [26,27] and does not affect particle collimation in our case. In contrast, an elongated magnetic field tunnel is generated when a high-density fast electron beam with a negative current (Figures 5D–F) is transported forward and plays a main role in collimating particle beams. The main reason is that a clockwise magnetic field surrounds the plasmas beam for a long time in a long size in space (see Figures 5G–I), which can efficiently collimate electrons in center (see Figures 5A–C). Meanwhile, that the electrons are restricted in the narrow region can improve the collimation of the accelerated ions.

Discussion

In the following section, the magnetic field effects on the collimation mechanism are described. It is well-known that the magnetic field is $\nabla \times B = \mu_0 j$, where μ_0 is the vacuum permeability and j is the current density. Usually, a quantitative estimate of the relationship between the current and magnetic fields can be obtained by employing a rigid beam model [28] to estimate the magnetic field generation, where a fixed current density is considered to vary with the radius. Here, the plasma beam with current is assumed to remain static. For simplicity, we used Gaussian profiles to fit the average current densities, where $j_x = j_0 \exp(-r^2/2R^2)$, j_0 is the maximum current density, and R is

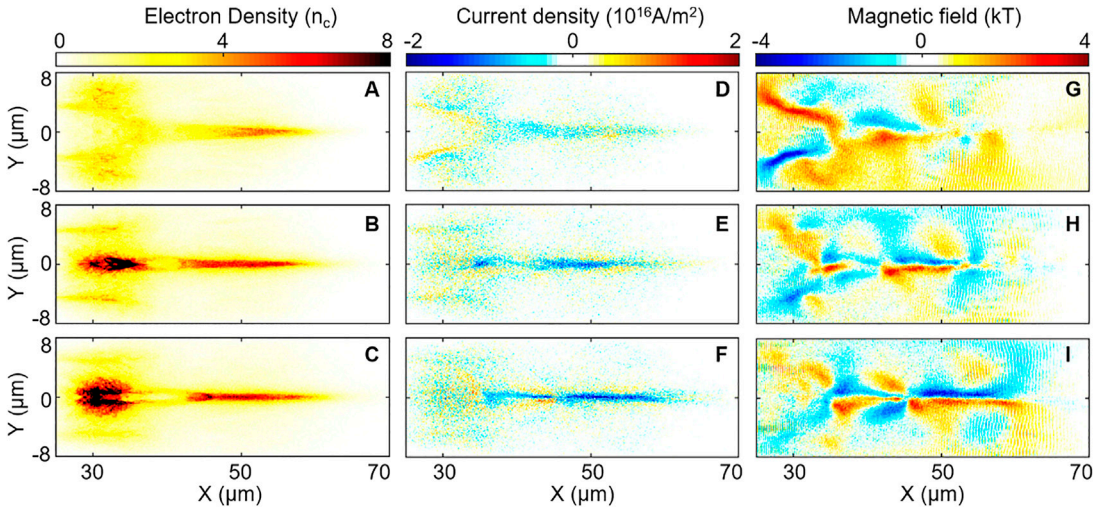

FIGURE 5
Collimation results driven by different topological structured LG lasers. Longitudinal cross sections of electron particle density ne **(A–C)**, current density **(D–F)**, and magnetic field **(G–I)** at t = 200TL for topological charge of laser l = 1 (top row), l = 2 (center row), and l = 3 (bottom row). For the current, the forward-moving electrons in the plasma beam defined here as a negative current are indicated in blue, whereas the positive current densities corresponding to the return current of the surrounding electrons are indicated in red.

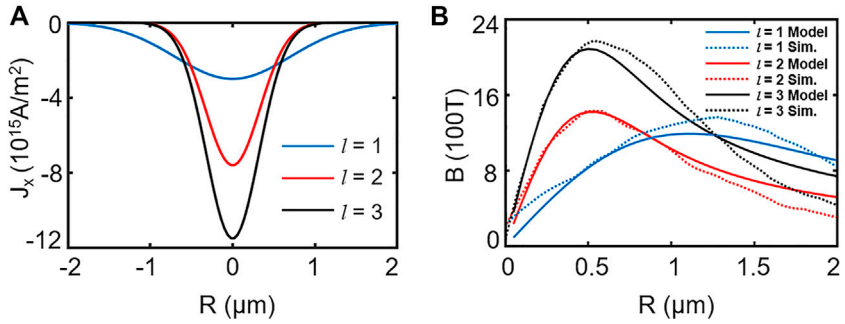

FIGURE 6
(A) Fitted current density distribution for the case of l = 1 (blue), l = 2 (red), and l = 3 (black). **(B)** The magnetic field in the rigid beam model calculation (solid line) and simulations (dotted line) for the case of l = 1 (blue), l = 2 (red), and l = 3 (black).

the current radius. In our simulations, $j_0 = 3 \times 10^{15}$A/m^2 (R = 0.7 μm), 7.6×10^{15}A/m^2 (R = 0.33 μm) and 11.5×10^{15}A/m^2 (R = 0.32 μm) are fitted and obtained at $t = 200T_L$ for the case of l = 1, 2, and 3, just as shown in Figure 6A. Evidently, a larger current density is generated for a larger l because more electrons are trapped by the topological intensity distributions of the LG lasers into the center region in the cases of l = 1 and 2 in the hole-boding stage. The magnetic field generation can then be obtained by integrating the current density, $B_\varphi = \frac{\mu_0}{2\pi}\frac{\int j_x ds}{r}$. Evidently, the magnetic fields calculated by the rigid beam model were almost consistent with the simulation results, as shown in Figure 6B.

The electrons can then be collimated in a quasistatic magnetic field with intensity B and radius L_r. Electrons with divergence θ, speed v, and the Lorentz factor γ can be confined and collimated in the magnetic field when the condition $L_r \geq r_e(1 - \cos\theta)$ [29] is satisfied, where $r_e = \gamma m_e v/eB$ is the electron Larmor radius. According to the Larmor radius, the corresponding relation can be obtained as

$$\Gamma < 2BL_r e/m_e \tag{3}$$

where $\Gamma = \gamma v\theta^2$. It is assumed that more electrons can be collimated when the strength of the magnetic field B increases according to Eq. 3. Based on the simple analysis and results, the

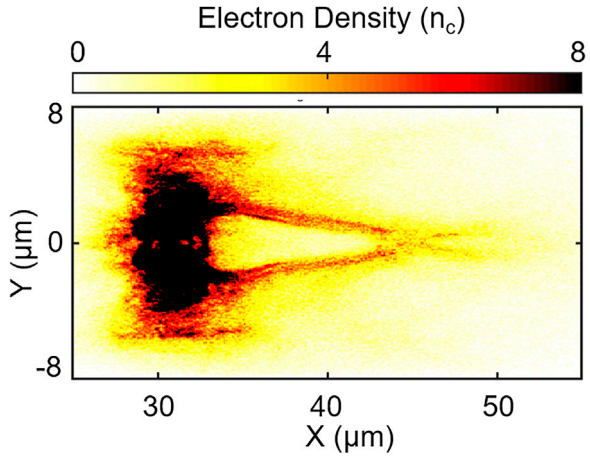

FIGURE 7
Longitudinal cross sections of electron density at $t = 160T_L$ for topological charge of laser $l = 5$.

beam collimation can be enhanced for $l = 3$ compared with the cases of $l = 1$ and 2, because B is larger in Figure 5B, which is consist with the simulation results in Figures 5A–C. It should be noted that the electrons and protons move together as a neutral plasma. Hence we just give the density distribution of electrons at $t = 400T_L$ (see Figure 5).

The collimation of the plasma beams disappears with an increase in the topological parameter l for the LG laser. For the example of $l = 5$, the electrons cannot be well collimated in a long-size tunnel $t = 160T_L$ as the case in Figure 7, although they are focused onto a spot at $x = 45$ μm. This is mainly because the intensity is smoothly distributed near the beam axis ($r = 0$), resulting in a small ponderomotive force at the center and weak concentrating effects on the plasma beam.

Conclusion

The self-collimation mechanism of an energetic plasma beam driven by an ultra-intense and ultrashort LG laser was demonstrated by 3D PIC simulation. A narrow plasma beam was formed and collimated to hundreds of nanometers and transported for a long time. On the one hand, the radial ponderomotive force of the LG laser can first concentrate the plasma into the center. On the other hand, such a beam can be further self-collimated by a magnetic field tunnel for a longer time. Studies have shown that better collimation can be achieved by properly choosing the topological charge l of an LG laser. It is important to achieve a better collimation effect and stable magnetic field when $l = 3$. The proposed scheme provides a simple and effective method for generating a collimated plasma beam and magnetic tunnel, which is useful in many applications, such as fast ignition in inertial confinement fusion, medical therapy, and astrophysics.

Data availability statement

The original contributions presented in the study are included in the article/Supplementary Material, further inquiries can be directed to the corresponding author.

Author contributions

HD conducted the simulations and drafted the manuscript. WW supervised the work. All authors discussed the results and reviewed the manuscript.

Conflict of interest

The authors declare that the research was conducted in the absence of any commercial or financial relationships that could be construed as a potential conflict of interest.

Publisher's note

References

1. Tiwari G., Gaul E., Martinez M., Dyer G., Gordon J., Spinks M., et al. Beam distortion effects upon focusing an ultrashort petawatt laser pulse to greater than 10^{22} W/Cm^2. *Opt Lett* (2019) 44(11):2764. doi:10.1364/ol.44.002764

2. Yoon J. W., Kim Y. G., Choi I. W., Sung J. H., Lee H. W., Lee S. K., et al. Realization of laser intensity over 20^{23} W/Cm^2. *Optica* (2021) 8(5):630. doi:10.1364/optica.420520

3. Roth M., Cowan T. E., Key M. H., Hatchett S. P., Brown C., Fountain W., et al. Fast ignition by intense laser-accelerated proton beams. *Phys Rev Lett* (2001) 86(3): 436–9. doi:10.1103/PhysRevLett.86.436

4. Xu H., Yu W., Yu M. Y., Cai H. B., Luan S. X., Yang S. H., et al. High energy density micro plasma bunch from multiple laser interaction with thin target. *Appl Phys Lett* (2014) 104(2):024105. doi:10.1063/1.4858956

5. Ramakrishna B., Kar S., Robinson A. P., Adams D. J., Markey K., Quinn M. N., et al. Laser-driven fast electron collimation in targets with resistivity boundary. *Phys Rev Lett* (2010) 105(13):135001. doi:10.1103/PhysRevLett.105.135001

6. Badziak J., Parys P., Rosiński M., Zaraś-Szydłowska A. Laser-driven accelerator of intense plasma beams for materials research. *Fusion Eng Des* (2017) 124: 1298–301. doi:10.1016/j.fusengdes.2017.01.061

7. Wang W. Q., Yin Y., Zou D. B., Yu T. P., Xu H., Shao F. Q. Effects of parameters on the proton focusing driven by coulomb explosion. *High Energ Density Phys* (2019) 32:77–81. doi:10.1016/j.hedp.2019.06.003

8. Zhuo H. B., Chen Z. L., Sheng Z. M., Chen M., Yabuuchi T., Tampo M., et al. Collimation of energetic electrons from a laser-target interaction by a magnetized target back plasma preformed by a long-pulse laser. *Phys Rev Lett* (2014) 112(21): 215003. doi:10.1103/PhysRevLett.112.215003

9. Stephens R. B., Snavely R. A., Aglitskiy Y., Amiranoff F., Andersen C., Batani D., et al. Kαfluorescence measurement of relativistic electron transport in the context of fast ignition. *Phys Rev E* (2004) 69(6):066414. doi:10.1103/PhysRevE.69.066414

10. Lancaster K. L., Green J. S., Hey D. S., Akli K. U., Davies J. R., Clarke R. J., et al. Measurements of energy transport patterns in solid density laser plasma interactions at intensities of 5×10^{20} W cm^{-2}. *Phys Rev Lett* (2007) 98(12):125002. doi:10.1103/PhysRevLett.98.125002

11. Kar S., Markey K., Simpson P. T., Bellei C., Green J. S., Nagel S. R., et al. Dynamic control of laser-produced proton beams. *Phys Rev Lett* (2008) 100(10): 105004. doi:10.1103/PhysRevLett.100.105004

12. Alraddadi R. A. B., Robinson A. P. L., Woolsey N. C. Improved fast electron transport through the use of foam guides. *Phys Plasmas* (2020) 27(9):092701. doi:10.1063/5.0011723

13. Robinson A. P., Sherlock M., Norreys P. A. Artificial collimation of fast-electron beams with two laser pulses. *Phys Rev Lett* (2008) 100(2):025002. doi:10.1103/PhysRevLett.100.025002

14. Kar S., Markey K., Borghesi M., Carroll D. C., McKenna P., Neely D., et al. Ballistic focusing of polyenergetic protons driven by petawatt laser pulses. *Phys Rev Lett* (2011) 106(22):225003. doi:10.1103/PhysRevLett.106.225003

15. Toncian T., Borghesi M., Fuchs J., d'Humieres E., Antici P., Audebert P., et al. Ultrafast laser-driven microlens to focus and energy-select mega-electron volt protons. *Science* (2006) 312(5772):410–3. doi:10.1126/science.1124412

16. Bacon E. F. J., King M., Wilson R., Frazer T. P., Gray R. J., McKenna P. High order modes of intense second harmonic light produced from a plasma aperture. *Matter Radiat Extremes* (2022) 7(5):054401. doi:10.1063/5.0097585

17. Wang W. P., Jiang C., Dong H., Lu X. M., Li J. F., Xu R. J., et al. Hollow plasma acceleration driven by a relativistic reflected hollow laser. *Phys Rev Lett* (2020) 125(3):034801. doi:10.1103/PhysRevLett.125.034801

18. Arber T. D., Bennett K., Brady C. S., Lawrence-Douglas A., Ramsay M. G., Sircombe N. J., et al. Contemporary particle-in-cell approach to laser-plasma modelling. *Plasma Phys Control Fusion* (2015) 57(11):113001. doi:10.1088/0741-3335/57/11/113001

19. Robinson A. P. L. Production of high energy protons with hole-boring radiation pressure acceleration. *Phys Plasmas* (2011) 18(5):056701. doi:10.1063/1.3562551

20. Wang W. P., Shen B. F., Zhang X. M., Ji L. L., Yu Y. H., Yi L. Q., et al. Dynamic study of a compressed electron layer during the hole-boring stage in a sharp-front laser interaction region. *Phys Rev ST Accel Beams* (2012) 15(8):081302. doi:10.1103/physrevstab.15.081302

21. Wang W. P., Shen B. F., Xu Z. Z. Accelerating gradient improvement from hole-boring to light-sail stage using shape-tailored laser front. *Phys Plasmas* (2017) 24(1):013104. doi:10.1063/1.4973330

22. Wang W. P., Shen B. F., Zhang X. M., Ji L. L., Wen M., Xu J. C., et al. Ultra-intense single attosecond pulse generated from circularly polarized laser interacting with overdense plasma. *Phys Plasmas* (2011) 18:083104. doi:10.1063/1.3623588

23. Wang W., Jiang C., Li S., Dong H., Shen B., Leng Y., et al. Monoenergetic proton beam accelerated by single reflection mechanism only during hole-boring stage. *High Pow Laser Sci Eng* (2019) 7(3):e55. doi:10.1017/hpl.2019.40

24. Forslund D. W., Shonk C. R. Formation and structure of electrostatic collisionless shocks. *Phys Rev Lett* (1970) 25(25):1699–702. doi:10.1103/PhysRevLett.25.1699

25. Snavely R. A., Key M. H., Hatchett S. P., Cowan T. E., Roth M., Phillips T. W., et al. Intense high-energy proton beams from petawatt-laser irradiation of solids. *Phys Rev Lett* (2000) 85(14):2945–8. doi:10.1103/PhysRevLett.85.2945

26. Borghesi M., MacKinnon A. J., Bell A. R., Gaillard R., Willi O. Megagauss magnetic field generation and plasma jet formation on solid targets irradiated by an ultraintense picosecond laser pulse. *Phys Rev Lett* (1998) 81(1):112–5. doi:10.1103/PhysRevLett.81.112

27. Stamper J. A., Papadopoulos K., Sudan R. N., Dean S. O., McLean E. A., Dawson J. M. Spontaneous magnetic fields in laser-produced plasmas. *Phys Rev Lett* (1971) 26(17):1012–5. doi:10.1103/PhysRevLett.26.1012

28. Davies J. R., Green J. S., Norreys P. A. Electron beam hollowing in laser–solid interactions. *Plasma Phys Control Fusion* (2006) 48(8):1181–99. doi:10.1088/0741-3335/48/8/010

29. Robinson A. P. L., Sherlock M. Magnetic collimation of fast electrons produced by ultraintense laser irradiation by structuring the target composition. *Phys Plasmas* (2007) 14(8):083105. doi:10.1063/1.2768317